Contents lists available at ScienceDirect

Colloids and Surfaces A: Physicochemical and Engineering Aspects

journal homepage: www.elsevier.com

Water-in-oil droplet formation in a flow-focusing microsystem using pressure- and flow rate-driven pumps

Sarah Lignel[a], Anne-Virginie Salsac[b, *], Audrey Drelich[a], Eric Leclerc[b, 1], Isabelle Pezron[a]

[a] Sorbonne Universités, Université de Technologie de Compiègne, Integrated Transformations of Renewable Material Laboratory (EA TIMR 4297 UTC-ESCOM), rue du Dr Schweitzer, 60200 Compiègne, France

[b] Sorbonne Universités, Université de Technologie de Compiègne – CNRS, Biomechanics & Bioengineering Laboratory (UMR CNRS 7338), rue du Dr Schweitzer, 60200 Compiègne, France

ARTICLE INFO

Keywords:
Flow-focusing microsystem
Monodisperse emulsion
Drop formation
Pressure controller
Flow-driven pump
Electronic–hydraulic analogy

ABSTRACT

Microfluidic flow-focusing systems are simple and cheap devices to produce monodisperse emulsions. The objective of the study is to determine the flow conditions to create water-in-oil emulsions with flow- and pressure-driven techniques, the use of pressure controllers becoming more systematic, owing to their high precision and capability to generate flows within a large range of fluid properties. The challenge is to make the link between applied pressures and flow rates to be able to switch from pressure to flow-rate driven systems (or vice-versa). To reach this purpose, we have derived a simple model using the electronic–hydraulic analogy between fluid transport in microchannels and electron transport in electric circuit. Thanks to the model, we show that droplets are generated in both cases within exactly the same range of values of inlet-to-outlet pressure differences (and thus flow rates). A unique diagram governs the production of an emulsion in the flow-focusing system. There exists a minimal value of the continuous flow under which no drops form, the outlet channel being occupied by a pure oil flow for all the disperse flow conditions. Above this limiting value, drops may be generated but only in a narrow range of disperse flow rate/pressure, the outlet channel being filled by a pure water flow above it. The state diagram shows that the drop formation regimes are governed by the continuous phase capillary number. The unified results provide the conditions needed to produce water-in-oil emulsion droplets and prove the great potential of the model to compare flow-driven and pressure-driven microfluidic experiments.

1. Introduction

The generation of emulsion droplets is commonly encountered in many industrial fields to produce paints, inks, agrochemicals, cosmetics, pharmaceutics or food products. If the formation of stable emulsions is desired in formulated products, it is undesired in other applications such as crude-oil production. Despite the large body of previous studies on emulsions [1–3], controlling emulsion stabilization and destabilization remains a major challenge, owing to a lack of understanding of their mechanisms, especially in the case of complex emulsions, such as the ones found in industry.

One of the key parameters to control is the droplet size distribution, as it influences the emulsion properties and their evolution in time. In the last decades, an increasing number of studies have involved microfluidic techniques: the objective has been to better understand the process of droplet formation in a controlled environment, and to determine how it depends on the circuit geometry and on the fluid parameters [4,5].

Microfluidics has also led to the emergence of many new technologies for drop generation [6]. It is a convenient technique to control multiple emulsions [7], chemical reactions [8] or monodisperse capsule production [9]. The microfluidic technologies that are classically used to generate stable and regular droplets are co-flowing streams, T-junctions, and flow-focusing devices [10,11]. In all three cases, the two fluid phases are driven through independent microchannels into a junction where the fluids come into contact with one another. Droplets are formed depending on the balance of the forces at stake: the kinetic force, drag force and buoyancy force exerted by the outer flow promote drop separation, while the interfacial tension force resists to it.

* Corresponding author.
Email address: a.salsac@utc.fr (A-V Salsac)
[1] Current address: LIMMS/CNRS IIS UMI 2820, Institute of Industrial Science, University of Tokyo, 4-6-1 Komaba, Meguro ku, 153-8505, Japan.

https://doi.org/10.1016/j.colsurfa.2017.07.065
Received 8 May 2017; Received in revised form 20 July 2017; Accepted 20 July 2017
Available online xxx
0927-7757/

Depending on the device geometry and flow conditions, different mechanisms of droplet formation can be obtained: squeezing, dripping or jetting [12–16]. Drops are directly produced in the squeezing and dripping regimes, while they form as a secondary process in the jetting regime, when the jet breaks up as a consequence of the Rayleigh-Plateau instability [4]. In the jetting regime, the drops are typically smaller in size than in the dripping regime for a same ejector tube.

Given a set of non-miscible fluids and a specific circuit, the challenge is to predict the experimental conditions needed to ensure the formation of droplets as well as their size. The thorough analysis of the process is very complex from a theoretical point of view. Scaling arguments are often used to establish diagrams of droplet formation regimes or to express the droplet size as a function of the experimental conditions [4,5,17–19]. Although the accuracy and capabilities of numerical simulations have greatly increased over the last decades, their resolution remains complicated for two-phase flows, particularly in the case of rectangular channels, such as the ones often used in microfluidic applications [20,21]. An additional difficulty in jetting arises from the fact that the drop formation is inherently linked to an instability phenomenon, which is by essence difficult to predict owing to its high sensitivity to perturbations. Most studies thus rely on experimental approaches.

In order to study the link between flow conditions and droplet size, there is the need to produce monodisperse emulsions. In most related studies reported in the literature, fluid flows are driven by flow-rate controlling devices, such as microsyringe pumps [22–26]. But nowadays, pressure-control systems are being used more and more frequently. Ward et al. [19] reported differences in the break-up process, but could not explain which phenomena may account for it.

The objective of the study is to determine the flow conditions to create water-in-oil emulsions with flow- and pressure-driven techniques and compare them. Water droplets dispersed in oil are produced in a flow-focusing geometry, in which the continuous oil phase is introduced in the two lateral channels of a trifurcation [17]. Diagrams of the flow regimes are drawn as a function of the applied flow rates or pressures depending on the case. In order to compare the two processes, a simplified model of the process is derived to relate pressure differences and flow rates using the analogy between the Hagen-Poiseuille and Ohm's law.

After having described the experimental setup and methods used to produce the emulsions in Section 2, we detail the model that relates pressure drops to flow rates in Section 3. We show in Section 4 that the model enables to obtain a unique diagram of the flow conditions for droplet formation and that the flow regimes are governed by the continuous phase capillary number.

2. Materials and methods

2.1. Fluid phases

The dispersed phase is deionised water, produced by a purification chain with a resistivity of 18 MΩ cm (Aquadem Veolia Water STI, Wissous, France). Its dynamic viscosity is $\eta_c = 1$ mPa s and its density $\rho_c = 1000$ kg m^{-3}. The continuous phase is paraffin oil (Carl Roth GmbH, Karlsruhe, Germany) mixed with 1.8% (w/w) of non-ionic lipophilic emulsifier in order to decrease the water/oil (w/o) interfacial tension and stabilize the emulsion droplets. The chosen emulsifier is sorbitan monooleate $C_{24}H_{44}O_6$ ($M_w = 428.6$ g mol^{-1}), also called Span® 80 (Aldrich Chemistry, Buchs, Switzerland). It has a low Hydrophilic Lipophilic Balance (HLB) of 4.3 promoting the formation of w/o emulsions [27]. Two grades of paraffin oil with low and high viscosity are used. Their dynamic viscosity η_ℓ was respectively measured to be 28 mPa s and 194 mPa s at 20 °C using an Anton Paar Rheometer (Graz, Germany), and their density ρ_ℓ was found to be equal to 850 kg m^{-3} and 880 kg m^{-3}. We measured a w/o interfacial tension γ of 3.4 ± 0.4 mN m^{-1} at equilibrium for both oil phases comprising 1.8% (w/w) emulsifier; it was determined at 20 °C by the pendant drop technique with a Tracker tensiometer (Teclis, Longessaigne, France).

2.2. Microfluidic device

The microfluidic device is composed of a Y-shaped flow-focusing device (Fig. 1) made in polydimethylsiloxane (PDMS, Sylgard 184) using a photolithographic technique [28]. The dispersed phase is introduced through the central channel (width $W_d = 107$ μm, length $L_d = 6$ mm) and intersected by the continuous phase that flows through the two lateral channels (width $W_c = 234$ μm, length $L_c = 4$ mm). Downstream of the flow-focusing trifurcation, the central channel (width $W = 107$ μm, length $L = 4$ mm) is followed by a serpentine channel of width 300 μm and length 8 mm. All the channels have a uniform depth h of 112 μm. The droplets and suspending fluid are finally collected in a large collecting chamber that is 1 cm in length, 2 cm in width and about 3 mm in depth.

2.3. Experimental procedure

The fluid flows are generated by controlling either the flow rate with syringe pumps (Fig. 2a), or the pressure with pressure controllers (Fig. 2b). The experiments are performed under the constant tempera-

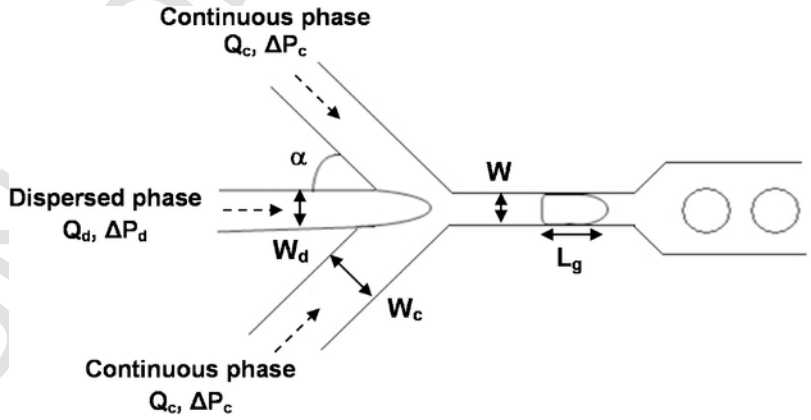

Fig. 1. Schematic drawing of the flow-focusing part of the microsystem.

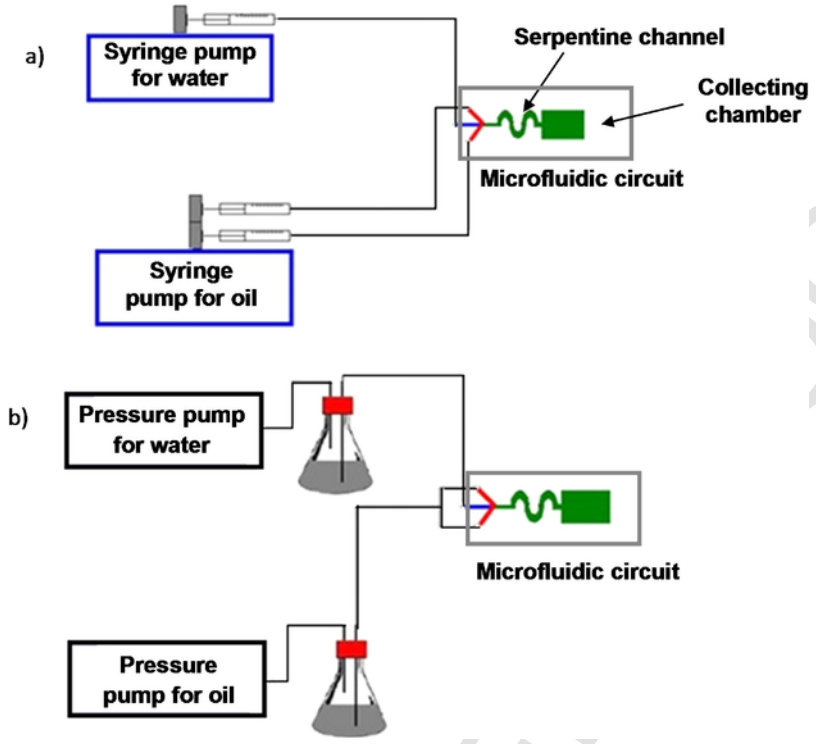

Fig. 2. Experimental set-up in the case of a flow generated in the microfluidic chip by a syringe-pump (a) or a pressure controller (b).

ture of 21 °C ± 0.2 °C. The microchannels are all contained in the same horizontal plane, so that gravitational effects can be neglected.

The main parameters that govern the drop formation are:

- The viscosity ratio η_d/η_c.
- The Weber number of the dispersed phase flowing in the central channel, which compares the inertial and capillary forces acting on it: $We_d = \frac{\rho_d W_d u_d^2}{\gamma}$.
- The capillary number of the continuous phase flowing in the lateral channels, which compares the viscous to the capillary forces acting on it: $Ca_c = \frac{\eta_c u_c}{\gamma}$.

2.3.1. Flow-driven mode

In the flow-rate driven mode, two syringe pumps with glass syringes of 1 mL capacity (Fisher Scientific, Illkirch, France) are used to generate the flow into the microfluidic device (Fig. 2a). The flow rates are varied between 0.1 and 5 mL h^{-1} in the central channel, and between 0.25 and 2 mL h^{-1} in the lateral channels. In order to determine the conditions required for the formation of water droplets and study the drop generation regimes, the flow rate Q_c is systematically increased by increments of 0.25 mL h^{-1}. For each set value of Q_c, the flow rate Q_d of the dispersed phase is then progressively increased to find the boundaries of the drop formation zone. Only the continuous phase with the low-viscosity oil could be employed with the syringe pump that was used. The flow conditions used in flow-driven mode correspond to a Weber number of the dispersed phase We_d ranging from 2.10^{-4} to 0.4, a capillary number of the continuous phase Ca_c ranging from 0.02 to 0.2, and Reynolds numbers that are below 0.1 for both phases. Stokes flow conditions can thus be assumed within the microfluidic channels.

2.3.2. Pressure-driven mode

In the pressure-driven mode, the oil and water flows are driven by two AF1 pressure pumps (Elveflow, Paris, France). The pressure of the continuous phase is varied from 0 to 1650 mbar with respect to the atmospheric pressure. The same pressure is guaranteed into the two lateral microchannels by connecting the tube coming out of the pressure controller to two identical tubes, each supplying a microchannel (Fig. 2b). The pressure of the dispersed phase is progressively increased in order to find the limits of the droplet formation region. Experiments are conducted with both the low- and high-viscosity oil phases.

2.3.3. Image recording

For the two flow-driven modes, data images are recorded at the trifurcation to visualize whether droplets are formed and to characterize their size. A Fastcam SA3 high-speed camera (Photron, Bucks, UK), mounted on a DMIL LED inverted laboratory microscope with LED illumination (Leica, Solms, Germany), is connected to a computer with the Photron FASTcam Version 318 program to record videos. Images of size 1024×512 pixels^2 are captured at 3800 frames per second (fps). The shutter speed is 1/75,000 s.

3. Model relating pressure differences in the circuit to flow rates

A relationship between pressure and flow rate in the circuit can be drawn from the analogy between electric circuits and microfluidic circuits [29,30]. Our purpose is to use the electronic-hydraulic analogy to evaluate the average flow rate in the different parts of the circuit for pressure-driven systems, in particular the flow rate of the fluids meeting at the junction, i.e. Q_d and Q_c, as they are the key parameters that control droplet formation.

In an electric circuit, the Ohm's law relates the voltage V across the conducting material (in Volt) to the current intensity I (in Amper), through the electric resistance R_E (in Ohm):

$$V = R_E I. \quad (1)$$

In the case of Stokes flow, the law of Hagen-Poiseuille similarly relates the pressure difference ΔP (in Pa) across a microfluidic channel to the fluid flow rate Q (in $m^3\ s^{-1}$), through the hydraulic resistance R_H

of the channel (Pa s m^{-3}):

$$\Delta P = R_H Q. \tag{2}$$

The pressure difference is thus analogous to the voltage and the flow rate to the current intensity. In order to derive the equations relating the pressure difference and flow rate, we represent the microfluidic circuit as a combination of the specific hydraulic resistances of the different channels (see Fig. 3 for the definition of the related symbols used for each of them).

The resistances are connected in parallel upstream of the trifurcation and in series downstream of it. We define R_{Heq} as the equivalent hydraulic resistance of the resistances R_{H0} and R_{HS} that are in series downstream of the trifurcation (see Fig. 3). The hydraulic resistance of a microfluidic channel depends on the fluid that flows through it and on the geometry of the channel. Upstream of the junction, the resistances R_{Hc} and R_{Hd} can be estimated from the infinite series that relates the flow rate of a single-phase fluid of viscosity η (in Pa s) to the pressure drop across a rectangular channel of length L (in m), characterized by a height h (in m) and width W (in m) of the same order of magnitude [5]. A good approximation of the formula is obtained, when retaining only the first term of the infinite series. The hydraulic resistance then reads

$$R_H = \frac{\Delta P}{Q} \approx \frac{12\eta L}{Wh^3\left(1 - 0.627\frac{h}{W}\right)}. \tag{3}$$

It must be noted that R_{Heq} cannot systematically be calculated using Eq. (3), since droplets may be present in the channel depending on the flow regime. In this case, its value has to be estimated from the experimental results.

We find the relationships between pressures and flow rates by applying Ohm's law and Kirchhoff's law to the equivalent electric circuit represented in Fig. 3:

$$\left\{\Delta P_d = P_d - P_s = R_{Hd}Q_d + R_{Heq}Q_0 \right. \tag{4}$$

$$\left\{\Delta P_c = P_c - P_s = R_{Hc}Q_c + R_{Heq}Q_0 \right. \tag{5}$$

$$\left\{Q_o = Q_d + 2Q_c \right. \tag{6}$$

From these expressions, relationships are deduced between the pressures drop ΔP_d and ΔP_c and the flow rates Q_d and Q_c of the single-phase fluids, respectively flowing through the central channel and the lateral channels before the junction:

$$\left\{\Delta P_d = \left(R_{Hd} + R_{Heq}\right) Q_d + 2R_{Heq}Q_c \right. \tag{7}$$

$$\left\{\Delta P_c = R_{Heq}Q_d + \left(R_{Hc} + 2R_{Heq}\right) Q_c \right. \tag{8}$$

The pressure-drop ratio is thus related to the flow rate ratio by:

$$\frac{\Delta P_d}{\Delta P_c} = \frac{2R_{Heq} + \left(R_{Hd} + R_{Heq}\right)\left(\frac{Q_d}{Q_c}\right)}{R_{Hc} + 2R_{Heq} + R_{Heq}\left(\frac{Q_d}{Q_c}\right)}. \tag{9}$$

Conversely, the relationships of the flow rates as a function of the pressure drops are:

$$Q_c = \frac{\left(\frac{R_{Hd}}{R_{Heq}} + 1\right)\Delta P_c - \Delta P_d}{\left(\frac{R_{Hd}R_{Hc}}{R_{Heq}}\right) + 2R_{Hd} + R_{Hc}}, \tag{10}$$

$$Q_d = \frac{\left(\frac{R_{Hc}}{R_{Heq}} + 2\right)\Delta P_d - 2\Delta P_c}{\left(\frac{R_{Hd}R_{Hc}}{R_{Heq}}\right) + 2R_{Hd} + R_{Hc}}. \tag{11}$$

Eqs. (9)–(11), evidence that no relation of proportionality exists between the pressure-drop ratio and flow-rate ratio. Droplet generation, therefore, does not follow the same behavior law, when expressed as a function of pressure drops or flow rates.

In order to figure out which sections of the circuit contribute the most to the hydraulic resistance, the resistances have been calculated for each of the microchannels using Eq. (3) assuming single-phase flow (Table 1).

The resistance R_{Heq} has also been determined to have a first estimate of its order of magnitude. It is of course only valid in the absence of droplet formation. The resistance of the lateral channels (R_{Hc}) and outlet channel (R_{H0} and R_{Hs}) is calculated for both the low- and high-viscosity paraffin, and that of the central channel prior to the junction (R_{Hd}) for water. Table 1 shows that the hydraulic resistance R_{Heq} beyond the trifurcation is dominant: the resistance of the central outlet channel (R_{H0}) is, indeed, significantly higher than the resistances of the inlet channels (R_{Hd} and R_{Hc}). If R_{Heq} is the predominant term in Eq. (9), one can expect that the pressure-drop ratio will be close to 1 for a large range of flow-rate ratios.

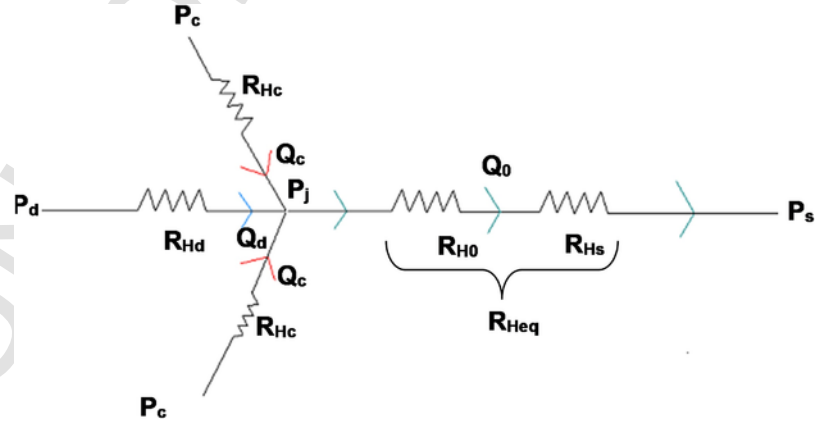

Fig. 3. Schematic representation of the microfluidic device as an electric circuit. R_{Hd} is the resistance of the central channel before the junction, R_{Hc} the resistance of the side channels, R_{H0} the resistance of the central channel after the junction, and R_{Hs} the resistance of the serpentine channel.

Table 1
Values of the hydraulic resistance considering single-phase flows.

	h (m)	L (m)	W (m)	Hydraulic resistance R_H (10^{12} SI)		
				Water (1 mPa s)	Oil (28 mPa s)	Oil (194 mPa s)
R_{Hd}	0.000112	0.006	0.000107	**1.39**		
R_{Hc}	0.000112	0.004	0.000234		**5.81**	**40.2**
R_{H0}[a]	0.000112	0.004	0.000107		**26.0**	**180**
R_{Hs}[a]	0.000210	0.008	0.000335		**1.25**	**8.65**
R_{Heq}[a]					**27.25**	**188.65**

[a]Calculated in absence of droplets.

4. Flow conditions for droplet formation using pressure- and flow-rate driven systems

When running the experiments, three distinct regimes are observed depending on the values of pressure drop and flow rate imposed to the dispersed phase (water):

- At very low Q_d or ΔP_d: the water inlet flow is not strong enough to penetrate the oil flow and no droplet formation is observed,
- At intermediate conditions: water droplets can be generated through dripping or jetting mechanisms depending on the pressure drop or flow rate imposed to the continuous phase (oil),
- At high Q_d or ΔP_d: the water inlet flow is too strong to be broken by the oil phase, resulting in an unbroken water flow with no droplet formation.

To control the process of droplet formation and generate emulsions with well-defined size distributions, we have explored in details the conditions required for droplet formation.

4.1. Flow-rate driven experiments

Flow-rate driven flows have solely been conducted with the low-viscosity oil, the higher viscosity oil leading to irregularities in the pump speed as well as leakage. Within the range of flow rates achievable by the syringe pump, droplet formation could only be observed within the dripping regime: no jetting was noted, even for the 2.2 mL h^{-1} flow rate, which corresponded to the syringe limiting capacity.

From these experiments, we extracted the range of flow rates enabling the formation of droplets. The corresponding region is delimited by dotted lines on the flow diagram shown in Fig. 4.

When the oil flows at flow rates lower than Q_c = 0.35 mL h^{-1}, no regular droplet formation is possible (left part of Fig. 4). Above this value, water droplets may form but only in a small range of water and oil flow rates. For every oil flow rate Q_c, there exists a critical value of the water flow rate Q_d, below which no water may flow downstream of the trifurcation (broken line at the bottom of Fig. 4). Above this value, conditions are reached for the water flow to be broken up by the oil flow, and water droplets are released in a periodical manner in the outlet channel. The dripping regime is observed up to an upper limiting water flow rate value (upper broken line in Fig. 4), which is found to vary from 2 to 3.75 mL h^{-1} when the oil flow rate Q_c is increased from 0.35 to 2.2 mL h^{-1}.

The size of the droplets was determined in the serpentine channel (see pictures in Fig. 4). For constant water flow Q_d, the droplet diameter decreases when increasing the oil flow rate Q_c. It, however, increases when the water flow rate Q_d is increased under a fixed Q_c. In the present experiments, the drop diameter ranges from 60 to 180 μm.

When the flows are driven by the pressure controllers, both dripping and jetting are observed as well as the transitory regime in-between. A thorough and extensive investigation of the droplet generation process in the different flow regimes is therefore possible contrary to the flow-rate driven case, where only dripping could presently be observed. The regime diagram represented in Fig. 5 shows images of droplet formation at the junction (dripping mode) or further downstream in the outlet channel, when it occurs at the extremity of the jet (jetting mode). The results show that below a limit oil pressure drop ΔP_c = 50 mbar, no droplet formation is possible. Above this limiting value, there exists a small range of ΔP_d, for which drops form for every value of ΔP_c.

When the water pressure drop (ΔP_d) reaches a value which is slightly below the oil pressure drop (ΔP_c), water droplets start forming, but droplets are only generated within a very narrow range of applied

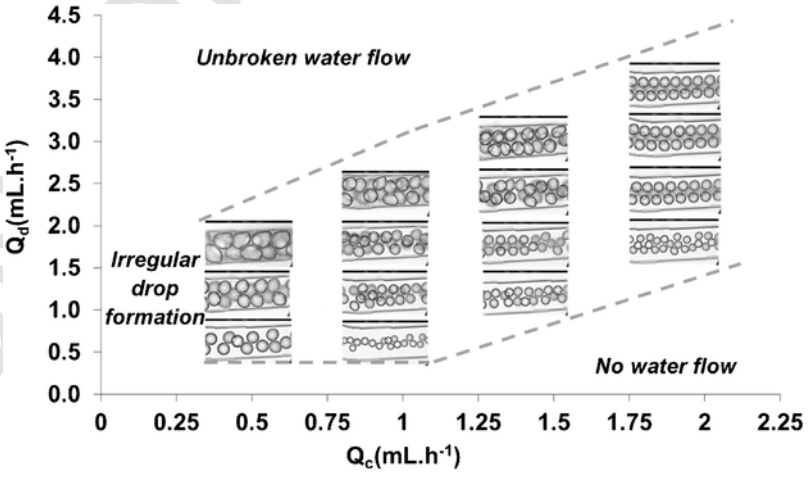

Fig. 4. Flow regime diagram in the flow-rate driven mode for the 28 mPa s low-viscosity oil.

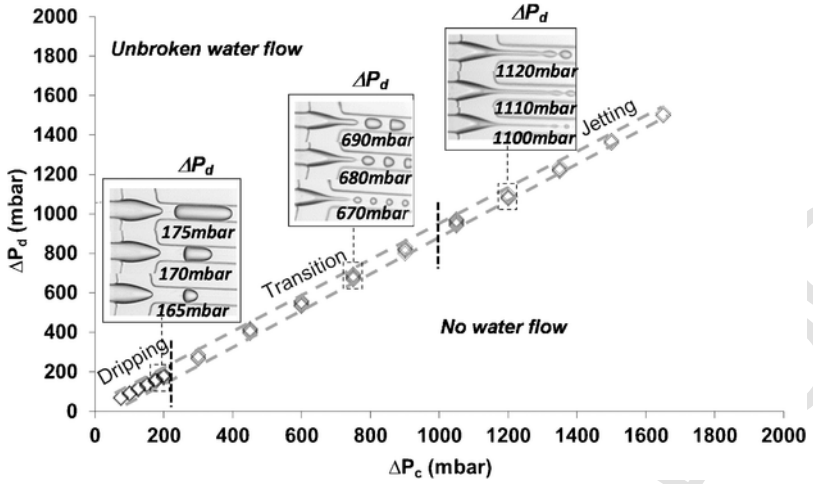

Fig. 5. Flow regime diagram in the pressure-driven mode for the 28 mPa s low-viscosity oil.

water pressure of the order of 10–20 mbar (Fig. 5). Outside this range, no droplet can form: below, pure oil flows through the outlet channel; above, water flows steadily without being broken up by the oil flow.

When compared to flow-rate driven mode, the generation of droplets appears to be even more sensitive to the conditions in the central channel. Within the drop formation region, dripping occurs up to $\Delta P_c \approx 220$ mbar. Above, a water jet starts forming intermittently downstream of the trifurcation with large variations over time: it is the transitory regime. Increasing the pressure results in the lengthening, thinning, and persistency of the jet over a longer period of time. Above the threshold value $\Delta P_c \approx 1000$ mbar, a stable jetting regime occurs. The water jet then reaches lengths up to several hundreds of micrometers and widths of a few tens of micrometers.

Before studying in detail in the next subsection the evolution of droplet size with the flow conditions, one can deduce from Fig. 5 that similar droplet sizes are found in the dripping regimes as in the flow-driven case (Fig. 4). The overall droplet size range is, however, extended towards lower values (40–170 μm), droplets being smaller in the jetting than in the dripping regime. In the jetting regime, droplet formation is indeed due to the rupture of the jet under the Rayleigh-Taylor instability. When ΔP_c increases, the droplet size decreases and tends towards the value predicted by the stability analysis of Kitamura et al. [31], which is about twice the jet diameter – see also Sandulache et al. [32].

A comparable zone of droplet formation is measured for the high-viscosity oil (data not shown). Only the ΔP_c threshold value between the transition and jetting regimes changes slightly with the oil viscosity. It is found to be around 1000 mbar for the low-viscosity oil (Fig. 5), and around 1300 mbar for the high-viscosity oil.

4.2. Comparison between flow- and pressure-driven experiments

In order to link the two flow regime maps (Figs. 4 and 5), one has to resort to the model presented in Section 3. The hydraulic resistance R_{Heq} of the fluid downstream of the junction, which corresponds to the resistance of a two-phase flow, is a priori not known and has to be estimated from the experimental results. To evaluate this parameter, we compare the formation of droplets within the dripping regime in both the pressure- and flow-driven modes for the low oil viscosity (28 mPa s). We have chosen to compare, in particular, the length L_g of the squeezed droplet. This length, normalized by the central channel depth h, is plotted in Fig. 6a and b as a function of the applied flow-rate and pressure ratio, respectively.

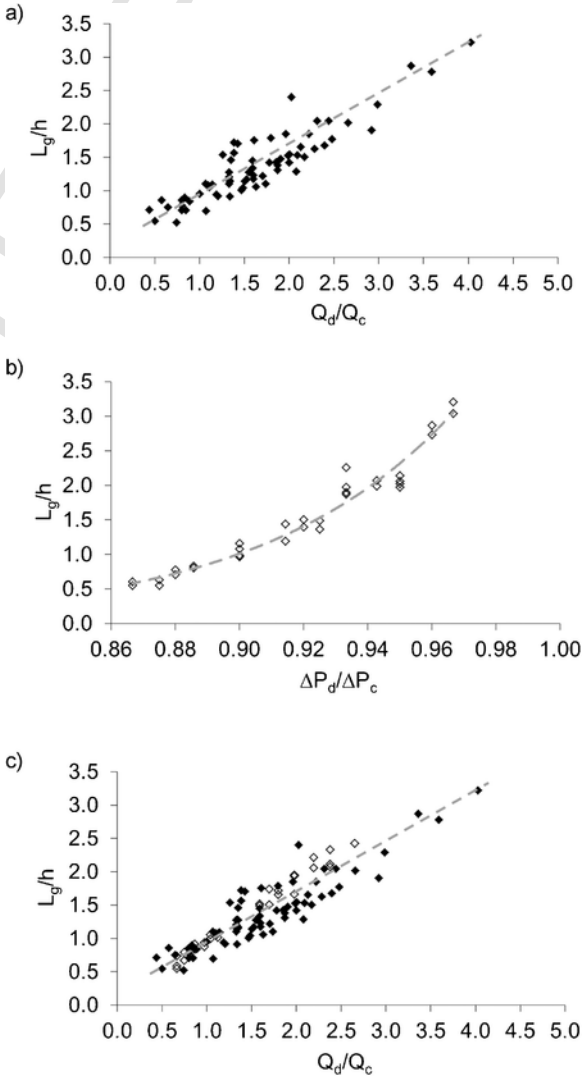

Fig. 6. Droplet length normalized by the channel depth h for the low-viscosity oil as a function of a) the flow rate ratio (syringe pumps), b) the applied pressure ratio (pressure pump device), c) Superposition of the values plotted as a function of the flow rate ratio (open dots correspond to pressure-driven experiments) obtained using Eq. (9) with $R_{eq} = 10^{13}$ (SI).

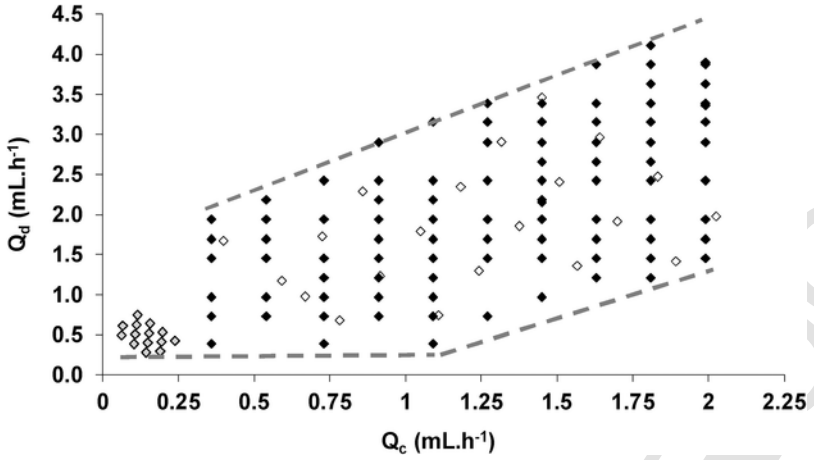

Fig. 7. Flow regime diagram in the dripping regime. Black diamonds: flow-rate driven mode (low-viscosity oil). Open diamonds: pressure-driven mode (low-viscosity oil). Grey diamonds: pressure-driven mode (high-viscosity oil).

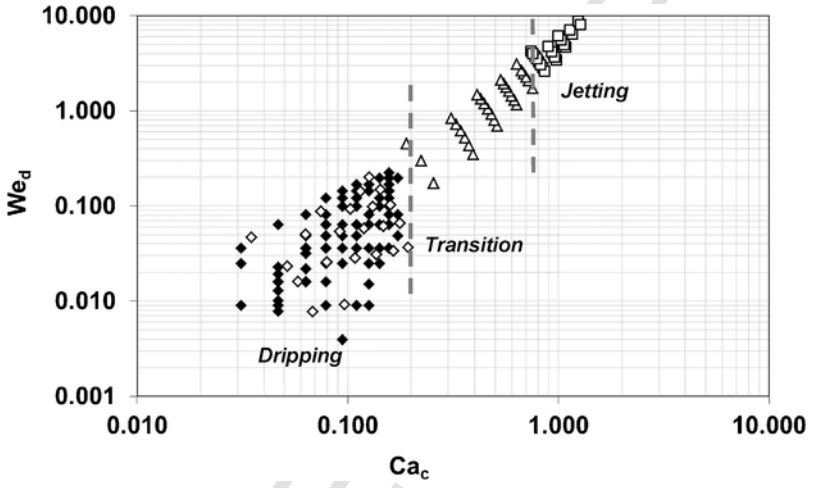

Fig. 8. State diagram of the flow regimes as a function of the disperse phase Weber number and continuous phase capillary number (low-viscosity oil): dripping (diamonds), transition (triangles), jetting (squares). Pressure-driven mode (white symbols). Flow rate-driven mode (black symbols). Dotted lines are a guide to help readers visualize the boundaries separating the drop formation regimes.

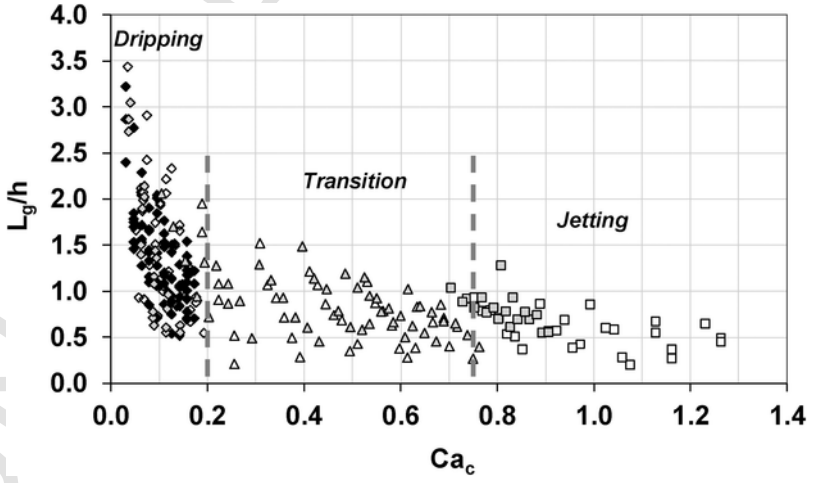

Fig. 9. Normalized droplet length as a function of the continuous phase capillary number in the dripping (diamonds), transition (triangles) and jetting (squares) regimes. Pressure-driven mode: low-viscosity oil (white symbols), high-viscosity oil (grey symbols). Flow rate-driven mode: low-viscosity oil (black symbols). Dotted lines are a guide to help readers visualize the boundaries separating the drop formation regimes.

In the case of the flow-driven mode, the droplet length has a linear dependency on the flow rate ratio. L_g/h varies between 0.5 and 3.5 when the flow-rate ratio is increased from approximately 0.5–4. Similar results of drop size ratios and linearity with the flow rate ratio have been obtained by He et al. [17]. Interestingly, the linear dependency had also been observed by Garstecki et al. [4] for a T-junction. Pressure-driven experiments lead to a similar range of normalized droplet length (pressure ratio varied within the narrow range 0.86–0.97). The difference is, however, that the length follows a non-linear evolution as a function of the applied pressure ratio (Fig. 6b).

We determine the value of R_{Heq} from Eq. (9) by finding the best superposition of L_g/h as a function of Q_d/Q_c for both sets of results (Fig. 6c). By doing so, we assume that R_{Heq} is constant and independent of the flow condition. The best fit is obtained for $R_{Heq} = 10^{13}$ (SI).

Knowing R_{Heq}, it is then possible to deduce the oil and water flow rates as a function of the applied pressures using Eqs. (10) and (11) for the pressure-controller results. The values obtained in the dripping regime are plotted in Fig. 7 and compared to the measurements in the flow-driven mode. The values fall in the same region of the map, and are in good agreement with the limits drawn in Fig. 4, which are reported here. The grey diamonds correspond to the values measured for the high-viscosity oil using the pressure controllers. The value of the hydraulic resistance R_{Heq} of the high-viscosity oil is calculated assuming a relationship of proportionality between the two-phase flow resistance and the oil phase viscosity. The hypothesis made is thus that the hydraulic resistance is mainly due to the friction of the continuous phase along the channel walls. A resistance $R_{Heq} = 6.9 \times 10^{13}$ SI is calculated for the 194 mPa s viscosity oil. Fig. 7 shows that the high-viscosity oil results enable to extend the study of the dripping regime to lower Q_c values.

5. Final discussion and conclusion

We have studied monodisperse emulsion production within a microfluidic flow-focusing system made of a trifurcation and investigated the inlet conditions necessary for drop generation, whether the flow is induced by a flow-driven system or a pressure-driven one. Pressure controllers are currently more and more used in microfluidics owing to their higher precision than flow-rate controlling devices such as syringe pumps. The latter face issues such as the finite fluid volume in the syringe and variabilities in flow whenever highly viscous flows or low flow rates are used. Resorting to glass syringes and to inner coatings (e.g. with proteins) may be a solution for some applications, but does not solve all the issues. This explains why experimentalists often use both flow- and pressure-driven systems within a same study. The question they face is how to convert the pressure differences into flow rates and vice-versa, which is needed to compare the results.

Our objective was to study the generation of monodisperse drops using a trifurcated microfluidic system and to propose a simple model to relate pressure difference ratios to flow rate ratios and convert the results obtained with both flow-generation techniques. The model that we have derived is based on the electronic–hydraulic analogy. Experimentally, we have injected water in the central branch and oil in the two lateral branches and investigated the range of inlet flow conditions required to generate a water-in-oil emulsion.

Similar results have been found in both sets of experiments (pressure-driven or flow-driven), namely that drops are only generated within a range of disperse flow rate Q_d (respectively, pressure difference ΔP_d for the pressure-driven experiments), the upper and lower values of which increase linearly with the continuous flow rate Q_c (respectively, pressure difference ΔP_c). Like Ward et al. [19], we observe a very high sensitivity to the inlet flow conditions in the case of the pressure-driven technique: droplets are only generated within a band of disperse pressure-differences that is not wider than 30 mbar in amplitude. The drop size thus experiences very large variations within a very narrow range of pressures ΔP_c.

If such a difference in flow condition extent range may surprise experimentalists when they move from flow-driven to pressure-driven systems, no difference in physical mechanisms are, however, found. After having translated the pressure values into their corresponding flow rate ones, one notices that both flow-generation systems result in exactly the same drop formation regimes and the same drop size. Fig. 7 proves the quasi-perfect correspondence in the regimes and in the upper/lower limiting values within which droplets form. This also proves that the model reproduces the governing physical phenomena, despite simplifying assumptions made in its derivation, and that determining the value of the equivalent hydraulic resistance of the microsystem branches with a two-phase flow from the experimental results is an adequate technique.

To finalize the study, we propose to express the results as a function of the non-dimensional numbers of the problem: the continuous phase capillary number Ca_c and the disperse phase Weber number We_d. We plot a phase diagram of the flow regimes in Fig. 8. To do so, the values of the capillary number Ca_c and Weber number We_d are calculated from the oil and water flow rates provided by Eq. (10). The state diagram reveals a very good coherence of the data whether the measurements are obtained using a pressure- or flow-driven system. It highlights that the transition between dripping and jetting flow regimes is governed mainly by the oil phase capillary number. In both cases, the dripping regime is obtained for capillary number Ca_c up to 0.2. The transition regime is found to occur for capillary numbers between 0.2 and ~0.75 and the jetting regime for capillary numbers larger than ~0.75. Like Utada et al. [7], we find that the end of the dripping regime occurs when the continuous phase capillary number is of the order of 0.2.

Since the transition is ruled by Ca_c, we plotted the normalized droplet length L_g/h as a function of Ca_c in Fig. 9. The drop size decreases with Ca_c when the regime transits from dripping to jetting. We observe the convergence towards a constant value at high Ca_c, as predicted by Kitamura et al. [31]. Within each regime, the droplet size is also influenced by the water phase Weber number: it is in the dripping regime that the effect is the largest, the disperse flow conditions strongly influencing the volume reached by the droplet at the time of detachment (Figs. 4 and 5). This phenomenon has, among others, been detailed by Sandulache et al. [32]. Additionally, the graph reinforces the very good agreement of the results whether they are obtained with a flow- or pressure-driven technique. The fact that a coherent unique state diagram could be derived from the two sets of experiments is made possible by the model. Without it, it would have been impossible to estimate the capillary number values from the pressure differences (when the pressure-induced system is used), and resorting only to the flow-induced systems would have prevented us from acquiring results in the transitional and jetting regimes, as well as comparing results for two oil viscosities. This proves that the model will be of great use to microfluidic experimentalists: it will enable them to relate pressure and flow rate values, and thus compare results obtained with flow-driven and pressure-driven techniques.

Acknowledgments

The European Space Agency is gratefully acknowledged for the financial support of the FASES (Fundamental and Applied Studies on Emulsion Stability) project. The authors would like to warmly thank Pr. Danièle Clausse, project leader for FASES at the Université de Technologie de Compiègne, for fruitful discussions. The French Ministry of Research is also acknowledged for the funding of Sarah Lignel PhD fellowship.

References

[1] D. Clausse, D. Daniel-David, F. Gomez, L. Komunjer, I. Pezron, C. Dalmazzone, C. Noik, Emulsion stability-application to complex emulsions of industrial interest, in: T.F. Tadros (Ed.), Colloid Stability and Application in Pharmacy, Wiley, New York, 2007, chap. 5.

[2] D.J. McClements, Emulsion design to improve the delivery of functional lipophilic components, Ann. Rev. Food Sci. Technol. 1 (2009) 241–269.

[3] G.G. Fuller, J. Vermant, Complex fluid–fluid interfaces: rheology and structure, Ann. Rev. Chem. Biomol. Eng. 3 (2012) 519–543.

[4] P. Garstecki, M.J. Fuerstman, H.A. Stone, G.M. Whitesides, Formation of droplets and bubbles in a microfluidic T-junction—scaling mechanism of break-up, Lab. Chip 6 (2006), 437–437.

[5] H.A. Stone, A.D. Stroock, A. Adjari, Engineering flows in small devices: microfluidics towards a lab-on-a-chip, Ann. Rev. Fluid Mech. 36 (2004) 381–411.

[6] G.M. Whitesides, The origins and the future of microfluidics, Nature 442 (2006) 368–373.

[7] A.S. Utada, E. Lorenceau, D.R. Link, P.D. Kaplan, H.A. Stone, D.A. Weitz, Monodisperse double emulsions generated from a microcapillary device, Science 308 (2005) 537–541.

[8] S.E. McCalla, A. Tripathi, Microfluidic reactors for diagnostics applications, Ann. Rev. Biomed. Eng. 13 (2011) 321–343.

[9] J.S. Kuo, D.T. Chiu, Controlling mass transport in microfluidic devices, Ann. Rev. Anal. Chem. 4 (2011) 275–296.

[10] C.N. Baroud, F. Gallaire, R. Dangla, Dynamics of microfluidics droplet, Lab. Chip 10 (2010) 2032–2045.

[11] G.F. Christopher, S.L. Anna, Microfluidics methods for generating continuous droplets streams, J. Phys. 40 (2007) R319–R336.

[12] H.A. Stone, Dynamics of drop deformation and breakup in viscous fluids, Ann. Rev. Fluid Mech. 26 (1994) 65–102.

[13] V. Cristini, Y.C. Tan, Theory and numerical simulation of droplet dynamics in complex flows: a review, Lab. Chip 4 (2004) 257–264.

[14] M. De Menech, P. Garstecki, F. Jousse, H.A. Stone, Transition from squeezing to dripping in a microfluidic T-shaped junction, J. Fluid Mech. 595 (2008) 141–161.

[15] T. Fu, Y. Ma, D. Funfschilling, C. Zhua, H.Z. Li, Squeezing-to-dripping transition for bubble formation in a microfluidic T-junction, Chem. Eng. Sci. 65 (2010) 3739–3748.

[16] J.H. Xu, S.W. Li, J. Tan, G.S. Luo, Correlations of droplet formation in T-junction microfluidic devices: from squeezing to dripping, Microfluid. Nanofluid. 5 (2008) 711–717.

[17] P. He, D. Barthès-Biesel, E. Leclerc, Flow of two immiscible liquids with low viscosity in Y-shaped microfluidic systems: effect of geometry, Microfluid. Nanofluid. 9 (2009) 293–301.

[18] Z. Nie, M.S. Seo, S. Xu, P.C. Lewis, M. Mok, E. Kumacheva, G.M. Whitesides, P. Garteski, H.A. Stone, Emulsification in a microfluidic flow focusing device: effect of the viscosities of the liquids, Microfluid. Nanofluid. 5 (2008) 585–594.

[19] T. Ward, M. Faivre, M. Abkarian, H.A. Stone, Microfluidic flow focusing: drop size and scaling in pressure-driven versus flow-rate-driven pumping, Electrophoresis 26 (2005) 3716–3724.

[20] P. Guillot, A. Adjari, J. Goyon, M. Joanicot, A. Colin, Droplets and jets in microfluidic devices, C. R. Chim. 12 (2009) 247–257.

[21] C. Zhou, P. Yue, J.J. Feng, Formation of simple and compound drops in microfluidic devices, Phys. Fluids 18 (2006) 092105.

[22] M.K. Mulligan, J.P. Rothstein, Scale-up and control of droplet production in coupled microfluidic flow-focusing geometries, Microfluid. Nanofluid. 13 (2012) 65–73.

[23] W. Lee, L.M. Walker, S.L. Anna, Role of geometry and fluid properties in droplet and thread formation in planar flow focusing, Phys. Fluids 21 (2009) 032103.

[24] W. van Hoeve, S. Gelke, J.H. Snoeijer, M. Versluis, M.P. Brenner, D. Lohse, Breakup of diminutive Rayleigh jets, Phys. Fluids 22 (2010) 12200.

[25] H.C. Shum, J. Varnell, D.A. Weitz, Microfluidic fabrication of water-in-water (w/w) jets and emulsions, Biomicrofluid6 (2012) 012808.

[26] M.L. Cordero, F. Gallaire, C.N. Baroud, Quantitative analysis of dripping and jetting regimes in co-flowing capillary jets, Phys. Fluids 23 (2011) 094111.

[27] A. Drelich, F. Gomez, D. Clausse, I. Pezron, Evolution of water-in-oil emulsions stabilized with solid particles, influence of added emulsifier, Colloids Surf. A 365 (2010) 171–177.

[28] T.X. Chu, A.V. Salsac, E. Leclerc, D. Barthès-Biesel, H. Wurtz, F. Edwards-Lévy, Comparison between measurements of elasticity and free amino group content for ovalbumin microcapsule membranes: discrimination of the cross-linking degree, J. Colloid Interface Sci. 355 (2011) 81–88.

[29] A. Biral, A. Zanella, Introducing purely hydrodynamic networking functionalities into microfluidic systems, Nano Commun. Netw. 4 (2013) 205–215.

[30] H.A. Stone, Introduction to fluid dynamics for microfluidic flow, in: H. Lee, D. Ham, R.M. Westervelt (Eds.), CMSO Biotechnology, Springer-Verlag, US, 2007, pp. 5–30.

[31] Y. Kitamura, H. Mishima, T. Takahashi, Stability of jets in liquid–liquid systems, Can. J. Chem. Eng. 60 (1982) 723–731.

[32] M.C. Sandulache, P. Paullier, R. Bouzerar, T. Yzet, O. Balédent, A.V. Salsac, Liquid injection in confined co-flow: application to portal vein embolization by glue injection, Phys. Fluids 24 (2012) 081902.